Available online at www.sciencedirect.com
ScienceDirect
Journal of Solid State Chemistry 180 (2007) 2209–2215
JOURNAL OF SOLID STATE CHEMISTRY
www.elsevier.com/locate/jssc

Crystal structure and phase transitions in perovskite-like $C(NH_2)_3SnCl_3$

Marek Szafrański[a,*], Kenny Ståhl[b]

[a]Institute of Physics, Adam Mickiewicz University, Umultowska 85, 61-614 Poznań, Poland
[b]Department of Chemistry, Technical University of Denmark, DK-2800 Lyngby, Denmark

Received 22 March 2007; received in revised form 15 May 2007; accepted 29 May 2007
Available online 3 June 2007

Abstract

X-ray single-crystal diffraction, high-temperature powder diffraction and differential thermal analysis at ambient and high pressure have been employed to study the crystal structure and phase transitions of guanidinium trichlorostannate, $C(NH_2)_3SnCl_3$. At 295 K the crystal structure is orthorhombic, space group *Pbca*, $Z = 8$, $a = 7.7506(2)$ Å, $b = 12.0958(4)$ Å and $c = 17.8049(6)$ Å, solved from single-crystal data. It is perovskite-like with distorted corner-linked $SnCl_6$ octahedra and with ordered guanidinium cations in the distorted cuboctahedral voids. At 400 K the structure shows a first-order order–disorder phase transition. The space group is changed to *Pnma* with $Z = 4$, $a = 12.1552(2)$ Å, $b = 8.8590(2)$ Å and $c = 8.0175(1)$ Å, solved from powder diffraction data and showing disordering of the guanidinium cations. At 419 K, the structure shows yet another first-order order–disorder transformation with disordering of the $SnCl_3^-$ part. The space group symmetry is maintained as *Pnma*, with $a = 12.1786(2)$ Å, $b = 8.8642(2)$ Å and $c = 8.0821(2)$ Å. The thermodynamic parameters of these transitions and the p–T phase diagram have been determined and described.

Keywords: Guanidinium trichlorostannate; Guanidinium cation; Perovskite; High pressure; Phase transition; Phase diagram; Rietveld refinement

1. Introduction

Perovskites and perovskite-like compounds form a numerous class of materials that are important both for fundamental and technological research. The high-temperature superconductors [1] and perovskite ferroelectric relaxors [2], known for their multiple applications, are the prominent, but far complete representatives of this group of materials. Many studies have been devoted to layered organic-based perovskite structures, whose properties can be tuned by varying the organic component and the perovskite matrix [3,4]. One of the characteristic features of perovskite crystals is a richness of phase transitions, as for instance displacive mechanisms arising from rotational distortions of the octahedral units forming the structures [5,6].

It is well known that many halide compounds adopt perovskite or perovskite-like structures [6,7]. This applies also to the crystals of the general formula AMX_3, where A stands for an organic/inorganic monovalent cation, M is a divalent metal and X denotes a halogen. Continuing our studies on guanidinium halides [8–13], we here describe the basic structural and thermodynamic properties of guanidinium trichlorostannate, $C(NH_2)_3SnCl_3$. This new member of the AMX_3 family crystallises in a distorted perovskite-like structure and undergoes a sequence of phase transitions as described in the following sections.

2. Experimental details

2.1. Synthesis

The $C(NH_2)_3SnCl_3$ crystals were synthesised by dissolving 0.3 mol of guanidinium chloride and 0.3 mol of stannous chloride in water. The substance was purified by repeated crystallisations from a water solution. A slow evaporation of the saturated solution at 295 K yielded colourless, good quality crystals, stable at ambient conditions.

*Corresponding author.
E-mail addresses: masza@amu.edu.pl (M. Szafrański), kenny@kemi.dtu.dk (K. Ståhl).

0022-4596/$ - see front matter © 2007 Elsevier Inc. All rights reserved.
doi:10.1016/j.jssc.2007.05.024

2.2. Differential thermal analysis (DTA)

Calorimetric measurements were carried out by DTA in the temperature range from 100 to 460 K. The sample in the form of pressed pellet of about 70 mg was heated/cooled at a temperature rate of 1 or 3 K/min. An indium standard was used for calibration of the calorimeter. The thermodynamic parameters of the phase transitions were determined with an accuracy of ±10%.

2.3. High-pressure DTA

The high-pressure studies were performed by DTA method in the pressure range up to 200 MPa. The pressure was generated by a GCA-10 Unipress compressor using a nitrogen gas as a transmitting medium. A manganin gauge ensured the pressure calibration with an accuracy of ±2 MPa. The DTA runs were measured at the temperature rate of 2 K/min. The temperature of the sample was measured by a copper–konstantan thermocouple mounted inside the high-pressure cell made of beryllium bronze. The transition temperatures used in the construction of p–T phase diagram were determined as the onsets of the thermal anomalies.

2.4. Single-crystal data collection, structure solution and structure refinement

A colourless crystal, $0.02 \times 0.12 \times 0.17\,mm^3$, was selected for the single-crystal data collection on a Siemens/Bruker SMART 1K CCD diffractometer with graphite monochromized Mo$K\alpha$ radiation at 295(1) K. A total of 24,395 reflections to $\theta_{max} = 34.0^\circ$ merged to 3223 unique reflections with $R_{int} = 0.033$ after absorption correction (SADABS [14]). The structure refined to $wR(F^2) = 0.063$, $R(F^2) = 0.026$ ($F > 2\sigma(F^2)$), $R(F^2) = 0.039$ (all data) and GOF = 1.03 using 92 parameters. Data collection and frame data integration were performed with programs SMART and SAINT [15], and structure solution and refinement with program SHELXTL [16]. Hydrogen positions were located in subsequent difference Fourier maps and initially refined freely. In the final cycles, the N–H distances were restrained to 0.87(2) Å and the isotropic thermal parameter set to 1.5 times that of the corresponding N atom. Final atomic parameters are given in Table 1a, and a selection of distances and angles in Table 2a.

2.5. High-temperature single-crystal study

The temperature dependence of the unit-cell parameters was in part studied on a KUMA-4 diffractometer with graphite monochromatized MoKα radiation. The single-crystal was fixed in a glass capillary and heated using a high-temperature attachment with a stream of air. The temperature was stabilized within ±0.5 K. The unit-cell dimensions were obtained by least-squares fits to 35 automatically centred reflections. In the high-temperature range, above 400 K, the measurements were hindered due to the breakdown of the single crystals at the phase transition.

Table 1a
Fractional coordinates and average isotropic temperature factor coefficients (U) for $C(NH_2)_3SnCl_3$ from single-crystal data at 295(1) K

	x/a	y/b	z/c	U (Å^2)
Sn	0.17058(2)	0.75936(1)	0.11922(1)	0.0360(1)
Cl(1)	0.39039(7)	0.76956(4)	0.22746(3)	0.0456(1)
Cl(2)	0.17349(8)	0.96429(5)	0.10629(4)	0.0570(2)
Cl(3)	0.41700(8)	0.74667(4)	0.02620(3)	0.0488(1)
C	0.6898(3)	1.0272(2)	0.13746(13)	0.0447(4)
N(1)	0.5894(3)	1.0095(2)	0.19563(12)	0.0619(5)
N(2)	0.7947(3)	1.1120(2)	0.13733(16)	0.0629(6)
N(3)	0.6814(4)	0.9612(3)	0.07890(17)	0.0898(9)
H(11)	0.534(4)	0.949(2)	0.1923(17)	0.093
H(12)	0.608(4)	1.047(3)	0.2361(13)	0.093
H(21)	0.793(4)	1.157(3)	0.1736(14)	0.094
H(22)	0.857(4)	1.119(3)	0.0983(14)	0.094
H(31)	0.604(4)	0.961(3)	0.0750(20)	0.135
H(32)	0.754(4)	0.970(4)	0.0431(18)	0.135

Spacegroup *Pbca*, $Z = 8$, $a = 7.7506(2)$ Å, $b = 12.0958(4)$ Å and $c = 17.8049(6)$ Å.

Table 1b
Fractional coordinates and isotropic temperature factor coefficients (U) for $C(NH_2)_3SnCl_3$ from powder diffraction data at 405(1) K

	x/a	y/b	z/c	U (Å^2)
Sn	0.7612(2)	0.2500	0.6949(3)	0.100(1)
Cl(1)	0.7240(6)	0.5527(5)	0.4102(5)	0.137(3)
Cl(2)	0.5577(5)	0.2500	0.7133(12)	0.153(4)
C	0.4995(35)	0.2500	0.2343(77)	0.124(9)
N(1)	−.0922(24)	0.2500	0.2307(33)	0.124(9)
N(2)	0.5676(34)	0.1668(33)	0.1752(54)	0.124(9)
N(3)	0.4689(33)	0.1025(29)	0.2359(68)	0.124(9)

Spacegroup *Pnma*, $Z = 4$, $a = 12.1552(2)$ Å, $b = 8.8590(2)$ Å and $c = 8.0175(1)$ Å.

2.6. Powder diffraction data collection

The powder diffraction data collections were performed at beamline I711 at the MAX-II synchrotron in Lund, Sweden [17]. The diffraction patterns were recorded with a Huber G670 powder diffractometer [18] equipped with a Huber G670.3 capillary furnace. The wavelength, 1.5226 Å, was determined using a Si standard. The powdered samples were contained in rotating 0.3 mm quartz capillaries and the data sets were accumulated for 3 min between 323 and 423 K in 5 K intervals. The patterns were recorded between 10° and 100° in steps of 0.005° in 2θ. The data sets were corrected for non-linearity by a built-in calibration routine. The background from the capillary and air scattering was subtracted from the data prior to data evaluation. The original diffraction patterns were retained and used for weighting in the subsequent Rietveld refinements. Final

Table 2a
Selected distances (Å) and angles (deg) for $C(NH_2)_3SnCl_3$ from single-crystal data at 295 K

Sn–Cl(1)	2.5752(5)	C–N(1)	1.313(3)
Sn–Cl(2)	2.4896(6)	C–N(2)	1.308(3)
Sn–Cl(3)	2.5326(6)	C–N(3)	1.315(3)
Sn–Cl(1)′	3.4905(5)		
Sn–Cl(2)′	3.7752(7)		
Sn–Cl(3)′	3.2515(6)		
Cl(1)–Sn–Cl(2)	90.89(2)	Cl(1)′–Sn–Cl(2)″	106.28(1)
Cl(1)–Sn–Cl(3)	89.62(2)	Cl(1)′–Sn–Cl(3)″	104.33(2)
Cl(2)–Sn–Cl(3)	89.60(2)	Cl(2)′–Sn–Cl(3)″	97.11(1)
N(1)–C–N(2)	119.8(2)		
N(1)–C–N(3)	119.8(2)		
N(2)–C–N(3)	120.4(3)		
H(11)···Cl(1)	2.52(2)	N(1)–H(11)···Cl(1)	161(3)
H(12)···Cl(1)	2.77(3)	N(1)–H(12)···Cl(1)	135(3)
H(21)···Cl(1)	2.64(2)	N(2)–H(21)···Cl(1)	148(3)
H(22)···Cl(3)	2.66(2)	N(2)–H(22)···Cl(3)	146(3)
H(31)···Cl(3)	2.62(2)	N(3)–H(31)···Cl(3)	162(4)
H(32)···Cl(2)	2.83(3)	N(3)–H(32)···Cl(2)	150(4)

Table 2b
Selected distances (Å) and angles (deg) for $C(NH_2)_3SnCl_3$ from powder diffraction data at 405 K

Sn–Cl(1) [*2]	2.464(5)	C–N(1)	1.15(5)
Sn–Cl(2)	2.476(7)	C–N(2) [*2]	1.21(5)
Sn–Cl(1)′ [*2]	3.550(5)	C–N(3) [*2]	1.36(3)
Sn–Cl(2)′	3.680(7)		
Cl(1)–Sn–Cl(1)	90.3(2)	Cl(1)′–Sn–Cl(1)′	98.1(2)
Cl(1)–Sn–Cl(2) [*2]	91.8(2)	Cl(1)′–Sn–Cl(2)′ [*2]	104.7(2)
N(1)–C–N(2) [*2]	140(3)		
N(1)–C–N(3) [*2]	74(2)		
N(2)–C–N(2)	75(4)		
N(2)–C–N(3) [*2]	141(4)		
N(2)–C–N(3) [*2]	67(3)		
N(3)–C–N(3)	148(5)		

atomic parameters at 405 K are given in Table 1b, and a selection of distances and angles in Table 2b.

The crystal data for the structures determined at 295 and 405 K, and experimental details have been deposited in the Cambridge Crystallographic Database Centre as supplementary publications CCDC 640983 and CCDC 640984, respectively.

3. Results and discussion

3.1. Calorimetric measurements

DTA measurements have shown that the $C(NH_2)_3SnCl_3$ crystals melt around 445 K. Two thermal anomalies characteristic of first-order phase transitions have been revealed below the melting point as illustrated in Fig. 1. On heating, the onsets were observed at $T_{32} = 400$–403 K and $T_{21} = 419$ K, while on cooling the anomalies occurred with a significant temperature hysteresis. The three phases of the crystal are referred to as phase I above T_{21}, phase II in the intermediate range of temperatures and

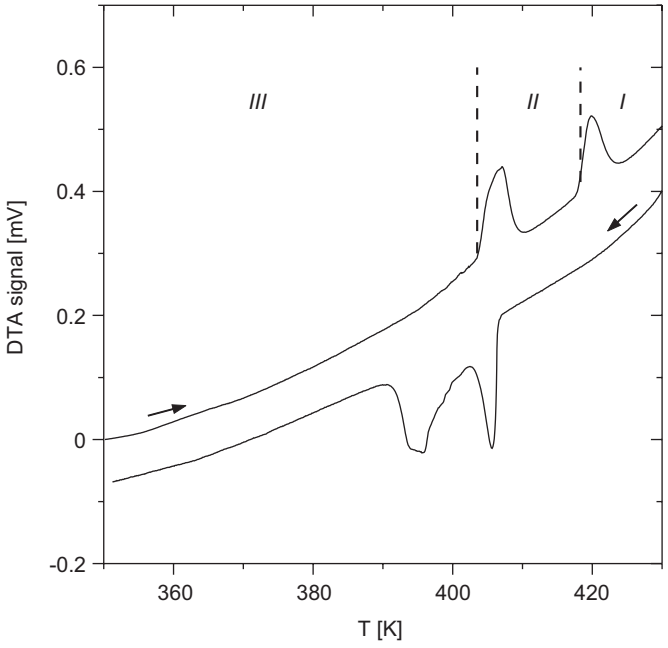

Fig. 1. DTA runs measured on heating and cooling the polycrystalline $C(NH_2)_3SnCl_3$ sample.

phase III below T_{32}. In order to avoid the overlapping of the signals, the measurements aimed at determination of the thermodynamic parameters of the transitions were performed at a relatively low rate of temperature changes of 1 K/min. The transition enthalpies and entropies, averaged from several DTA runs, are collected in Table 3. These parameters clearly indicate that both phase transitions involve an order–disorder contribution. Since the transition entropies are close to $R\ln 2$, a two- and a four-configurational disorder can be expected in phases II and I, respectively.

3.2. Thermal expansion of the crystal lattice

The first-order phase transition at T_{32} is associated with a strain that strongly affects the quality of single-crystals, resulting in broadening and splitting of reflections. Therefore the data collected, in several trials and using different crystals, above the transition temperature T_{32} were of rather poor quality and did not allow us to solve the single-crystal structure of phase II. Nevertheless, they proved that in the intermediate phase the crystals remained in the orthorhombic system. Fig. 2 shows the temperature dependences of the unit-cell dimensions as obtained from powder diffraction data in the temperature range 323–420 K. The lattice parameters change abruptly at T_{32}, consistent with the first-order character of the transition. As follows from Fig. 2 at T_{32} the crystal elongates along [100] by about 2.04% and contracts simultaneously along [001] by 1.28%, while its dimension along [010] remains almost unchanged. In consequence the crystal volume increases by 0.8% (see also Table 3). At T_{21} the unit-cell changes are minute. However, the

Table 3
Thermodynamic parameters of the phase transitions in $C(NH_2)_3SnCl_3$ (ΔT_{tr} denotes the temperature hysteresis)

Phase transition	T_{tr} (K)	ΔT_{tr} (K)	ΔH (kJ mol^{-1})	ΔS (J K^{-1} mol^{-1})	$\Delta V/Z$ (Å^3)	dT_{tr}/dp (K GPa^{-1})
II–I	419	10	1.74	4.2 (R ln 1.7)	0.76[a]	109.0
III–II	400–403	3–5	2.46	6.1 (R ln 2.1)	1.67	197.2

[a]Calculated from Eq. (3).

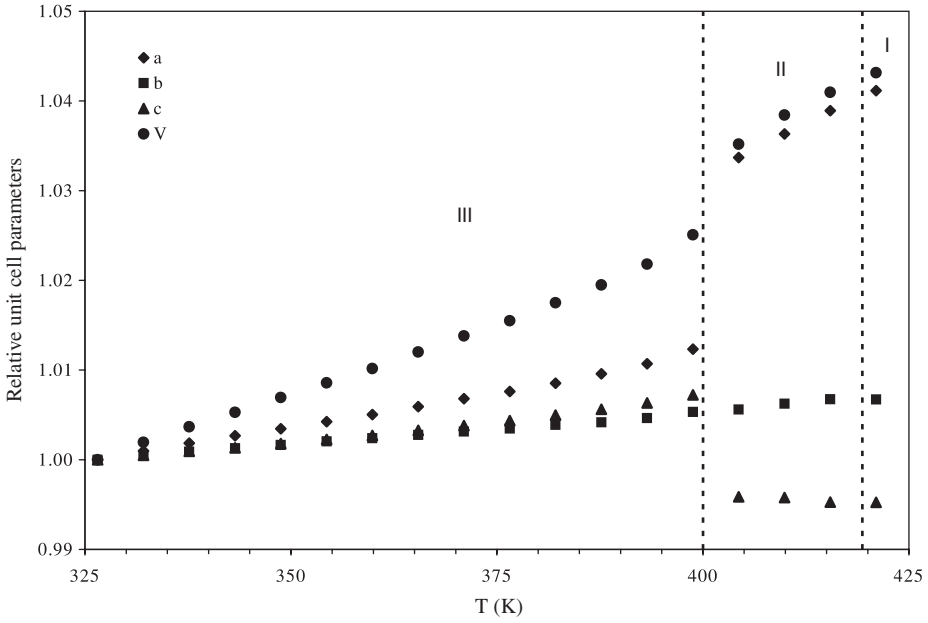

Fig. 2. Temperature dependence of the relative unit-cell parameters.

diffracted intensities change abruptly as demonstrated in Fig. 3a and b.

3.3. Crystal structures

3.3.1. Phase III, 295–400 K

The room-temperature crystal structure is built from planar guanidinium ions and pyramidal trichlorostannate(II) ions bound by electrostatic forces and N–H···Cl hydrogen bonds. If the tin coordination sphere is extended to next-nearest neighbours (Sn–Cl = 3.25–3.78 Å) its coordination can be described as distorted octahedral with the tin lone pair close to the centre of the octahedron. The distorted octahedra share corners and together with the guanidinium ions they form a perovskite-like structure (Fig. 4a). The guanidinium ions are well ordered and all their hydrogens are engaged in N–H···Cl hydrogen bonds with H···Cl distances in the range 2.52–2.83 Å (Table 2a) and N···Cl distances in the range 3.3–3.6 Å.

3.3.2. Phase II, 400–418 K

On heating to about 400 K, phase III transforms to phase II through an order–disorder transition. The crystal structure of phase II was solved from powder diffraction data. The original c-axis is cut into half and the space group changed to *Pnma* with $a_{II} = b_{III}$, $b_{II} = 1/2c_{III}$ and $c_{II} = a_{III}$. As seen from Figs. 4a and b, the transformation to phase II increases the symmetry by disordering of the guanidinium ion and placing the average ion in a more centred position in the distorted cubeoctahedral void. The refined N positions result in at least two N···Cl distances each in the range 3.3–3.8 Å, i.e., being potentially hydrogen bonded.

3.3.3. Phase I, 418–445 K

The crystal structure of phase I could not be solved in detail from powder diffraction data. The unit-cell variations follow the same trends as phase II, but the intensities show some abrupt changes at 420 K (cf. Figs. 3a and b). Space group extinctions are in full agreement with space group *Pnma*. Although a refinement starting from the phase II structure is possible, residual difference electron density indicates severe disorder in the Sn and Cl positions, which the present data could not resolve (Fig. 3b). Thus, phase I can be considered as closely related to phase II, but disordered both in guanidinium, Sn and/or Cl sites.

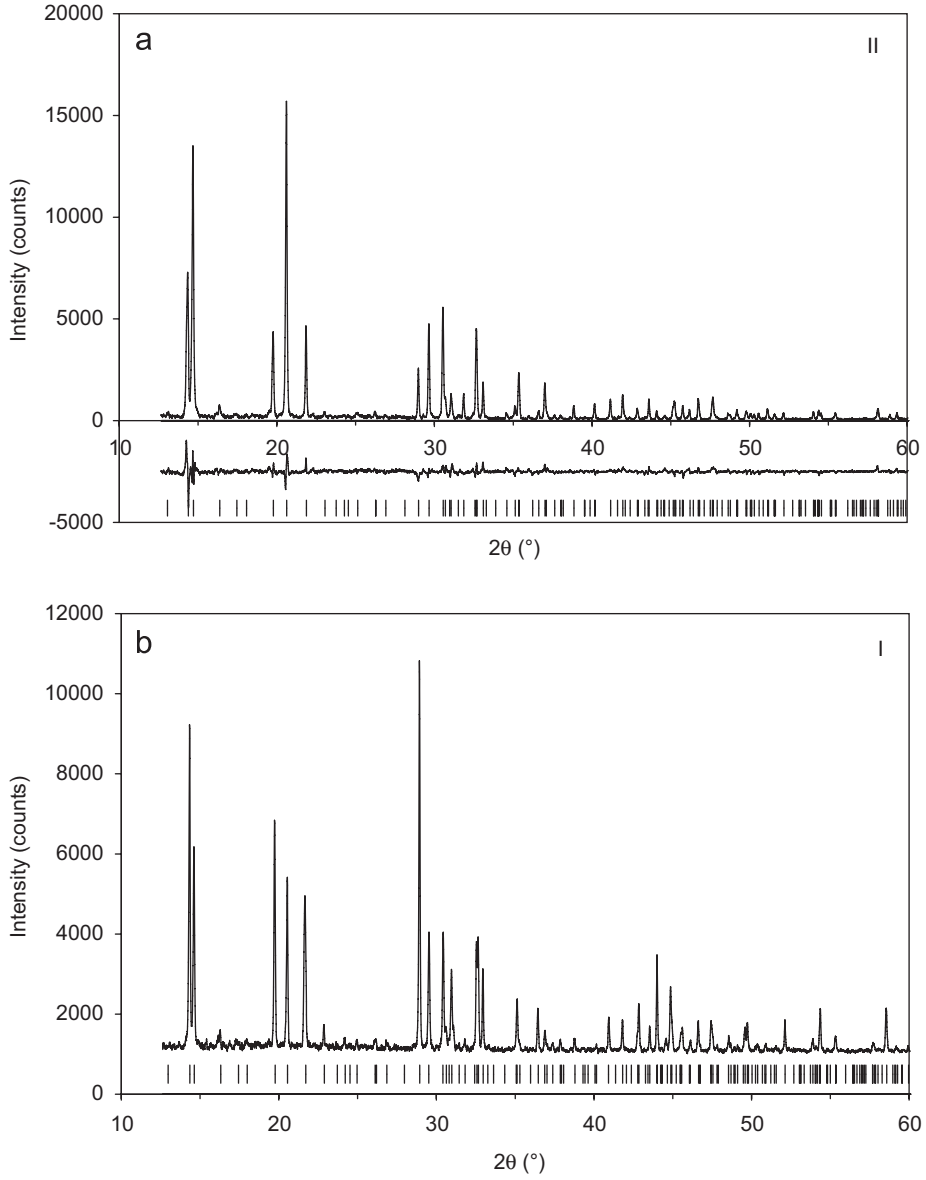

Fig. 3. (a) Rietveld fit for $C(NH_2)_3SnCl_3$ at 405 K, space group *Pnma*, $R_p = 16.8\%$, $wR_p = 15.3\%$, GOF = 1.54, $R_{Bragg} = 5.8\%$ from 8699 observations, 482 Bragg reflections and 34 refined parameters. (b) Powder diffraction pattern for $C(NH_2)_3SnCl_3$ at 420 K showing Bragg peak positions corresponding to space group *Pnma*, $a = 12.1786(2)$ Å, $b = 8.8642(2)$ Å and $c = 8.08214(2)$ Å.

3.4. *p–T* phase diagram

Owing to the parameters of our high-pressure cell, the *p–T* phase relations in $C(NH_2)_3SnCl_3$ were examined in the temperature range limited to 440 K. The transition temperatures were determined from the DTA heating runs. The results of the high-pressure measurements are plotted in Fig. 5. Both transition temperatures increase linearly with increasing pressure. The transition lines can be well fitted by the following equations:

$$T_{32}(p) = 399.9 + 0.1972p, \quad (1)$$

$$T_{21}(p) = 419.1 + 0.109p, \quad (2)$$

where temperature and pressure are expressed in K and MPa, respectively. These transition lines intersect at 219 MPa and 443 K, where the triple or other singular point can be expected. The pressure dependence of the first-order phase transition is described by the Claussius–Clapeyron equation:

$$\frac{dT}{dp} = \frac{\Delta V}{\Delta S}, \quad (3)$$

where ΔV and ΔS are the volume and entropy changes at the transition temperature, respectively. Applying Eq. (3), we estimated the change in the crystal volume at T_{21}. The magnitudes of ΔV_{21} and ΔV_{32}, collected in Table 3, point out that the crystal expansion at the transition

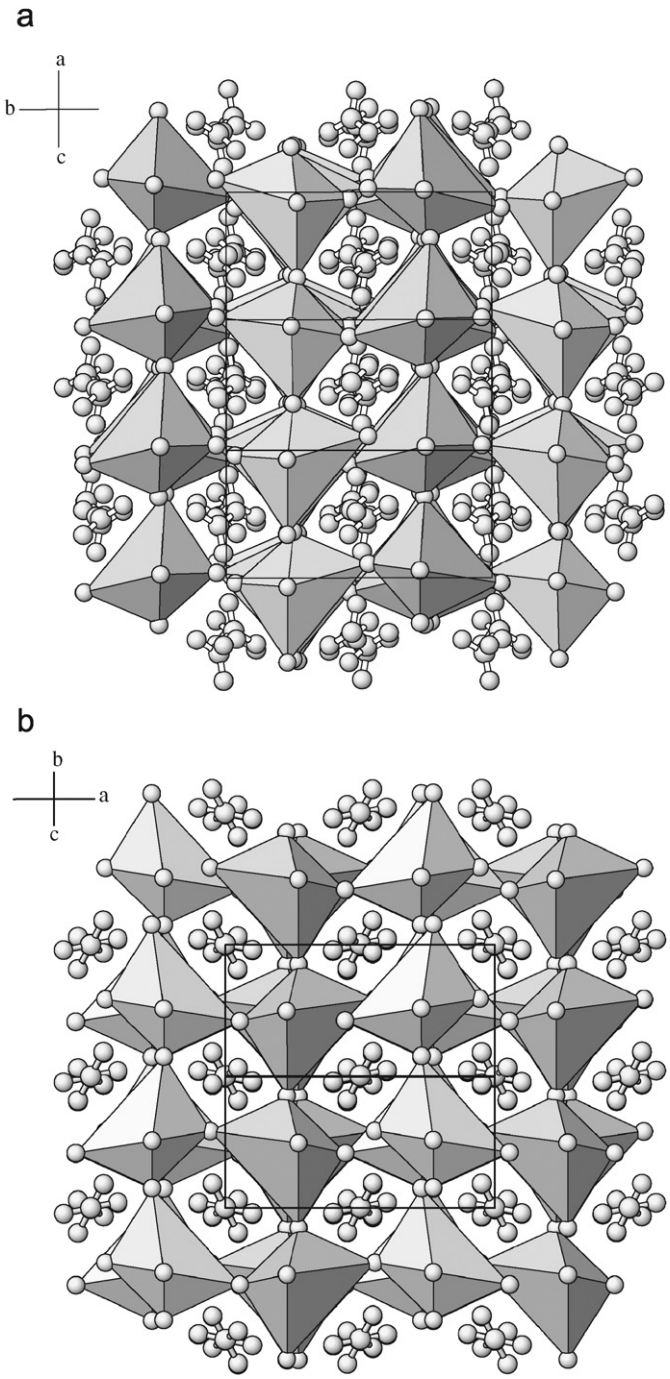

Fig. 4. Crystal structure of $C(NH_2)_3SnCl_3$ (a) at 295 K viewed down the (102) direction and (b) at 405 K viewed down the (011) direction.

between phases II and I is more than two times lower in comparison to the effect observed at the transition between phases III and II. Eq. (3) can also be used to calculate independently the transition entropy associated with the transition at T_{32}. The calculations yield $\Delta S_{32} = 5.8\,\mathrm{J\,mol^{-1}\,K^{-1}}$, which is in good agreement with the experimental value (cf. Table 3) determined from the DTA measurements.

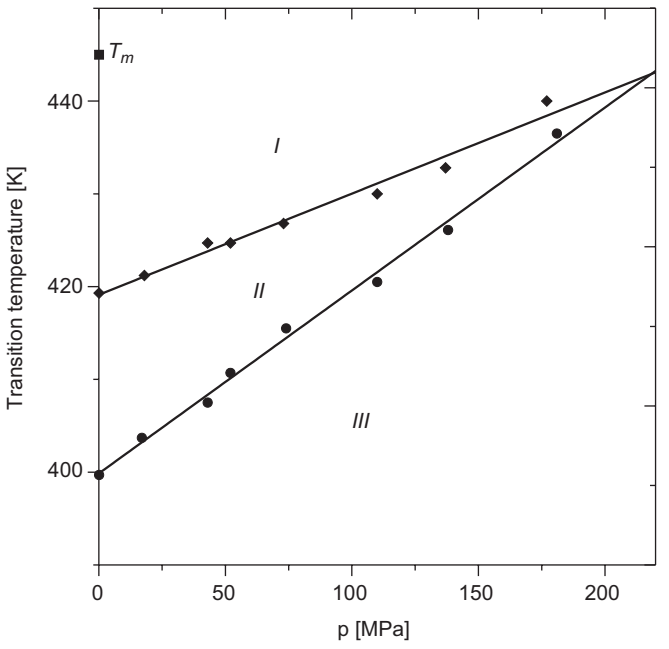

Fig. 5. The $p-T$ phase diagram of $C(NH_2)_3SnCl_3$, T_m denotes the melting point.

4. Conclusions

The characteristic feature of $C(NH_2)_3SnCl_3$ crystal is its perovskite-like structure with distorted cubeoctahedral voids occupied by the highly symmetric guanidinium cations. In the room-temperature phase III the positions of the cations in the voids are stabilised both by the non-symmetric potential and weak hydrogen bonds between N–H groups and chlorine atoms. The rise in temperature leads to a sequence of two order–disorder-type phase transitions. The transition between the phases III and II involves the two-configurational disordering of the cations and substantial changes in the cationic surrounding. An additional disordering occurs in the anionic sublattice of the crystal at the transition to the high-temperature phase I. The application of hydrostatic pressure reduces the interionic distances leading to the enhancement of electrostatic forces. This effect hinders the dynamic disordering of the ions, and hence the upward shift of the transition temperatures. Pressure affects both phase transitions in different ways, resulting in different pressure coefficients of their transition temperatures. In consequence, the transition lines meet at the singular point on the $p-T$ phase diagram. It is highly probable that at this point the mechanisms of the transitions become coupled and at higher pressures only one transition line exists, separating the low-temperature ordered and high-temperature disordered phases, but this problem requires further study. The pressure effect of a coalescence of two order–disorder phase transitions into a single one was observed previously in diguanidinium tetraiodoplumbate, $[C(NH_2)_3]_2PbI_4$ [12]. Such behaviour may be a characteristic feature for the organic–inorganic heterostructures, in which the

non-spherical organic units occupy the voids formed from the inorganic component.

Appendix A

Supplementary material (crystal data for the structures determined at 295 and 405 K) contain the supplementary crystallographic data for 640983 and 640984. These data can be obtained free of charge via http://www.ccdc.cam.ac.uk/conts/retrieving.html, or from the Cambridge Crystallographic Data Center, 12 Union road, Cambridge CB2 1EZ, UK; fax: (+44) 1223-336-033; or e-mail: deposit@ccdc.cam.ac.uk.

References

[1] J.G. Bednorz, K.A. Müller, Z. Phys. B 64 (1986) 189.
[2] G.A. Samara, Solid State Phys. 56 (2001) 239.
[3] D.B. Mitzi, C.A. Feild, W.T.A. Harrison, A.M. Guloy, Nature (London) 369 (1994) 467.
[4] G.C. Papavassiliou, Prog. Solid State Chem. 25 (1997) 125.
[5] D.M. Hatch, H.T. Stokes, K.S. Aleksandrov, S.V. Misyul, Phys. Rev. B 39 (1989) 9282.
[6] K.S. Aleksandrov, A.T. Anistratov, B.V. Beznosikov, N.V. Fedoseeva, Phase Transitions in Crystals of Halide ABX_3 Compounds, Nauka, Novosibirsk, 1981.
[7] K.S. Aleksandrov, N.V. Fedoseeva, I.P. Spevakova, Magnetic Phase Transitions in Halide Crystals, Nauka, Novosibirsk, 1983.
[8] M. Szafrański, Thermochim. Acta 307 (1997) 177.
[9] M. Kubicki, M. Szafrański, Acta Crystallogr. C 53 (1997) 1558.
[10] M. Kubicki, M. Szafrański, J. Mol. Struct. 446 (1998) 1.
[11] M. Grottel, M. Szafrański, Z. Pająk, Z. Naturforsch. 52a (1997) 783.
[12] M. Szafrański, A. Katrusiak, Phys. Rev. B 61 (2000) 1026.
[13] M. Szafrański, K. Ståhl, Phys. Rev. B 62 (2000) 8787.
[14] G.M. Sheldrik, SADABS. Program for Empirical Correction of Area detector Data. Version 2.01, University of Göttingen, Germany, 2000.
[15] Bruker SMART and SAINT-plus, Bruker AXS Inc., Madison, WI, USA, 1997–1999.
[16] G.M. Sheldrick, SHELXS97 and SHELXL97, University of Göttingen, Germany, 1997.
[17] Y. Cerenius, K. Ståhl, L.A. Svensson, T. Ursby, Å. Oskarsson, J. Albertsson, A.I. Liljas, J. Synchrotron Radiat. 7 (2000) 203.
[18] K. Ståhl, J. Appl. Crystallogr. 33 (2000) 394.